

UC San Diego

UC San Diego Previously Published Works

Title

Intestinal FXR agonism promotes adipose tissue browning and reduces obesity and insulin resistance

Permalink

<https://escholarship.org/uc/item/4sf2h363>

Journal

Nature Medicine, 21(2)

ISSN

1078-8956

Authors

Fang, Sungsoon

Suh, Jae Myoung

Reilly, Shannon M

et al.

Publication Date

2015-02-01

DOI

10.1038/nm.3760

Peer reviewed

Published in final edited form as:

*Nat Med.* 2015 February ; 21(2): 159–165. doi:10.1038/nm.3760.

## Intestinal FXR agonism promotes adipose tissue browning and reduces obesity and insulin resistance

Sungsoon Fang<sup>1</sup>, Jae Myoung Suh<sup>1</sup>, Shannon M Reilly<sup>2</sup>, Elizabeth Yu<sup>1</sup>, Olivia Osborn<sup>3</sup>, Denise Lackey<sup>3</sup>, Eiji Yoshihara<sup>1</sup>, Alessia Perino<sup>4</sup>, Sandra Jacinto<sup>1</sup>, Yelizaveta Lukasheva<sup>1</sup>, Annette R Atkins<sup>1</sup>, Alexander Khvat<sup>5</sup>, Bernd Schnabl<sup>3</sup>, Ruth T Yu<sup>1</sup>, David A Brenner<sup>3</sup>, Sally Coulter<sup>6</sup>, Christopher Liddle<sup>6</sup>, Kristina Schoonjans<sup>4</sup>, Jerrold M Olefsky<sup>3</sup>, Alan R Saltiel<sup>2</sup>, Michael Downes<sup>1</sup>, and Ronald M Evans<sup>1,7</sup>

<sup>1</sup>Gene Expression Laboratory, Salk Institute for Biological Studies, La Jolla, California, USA <sup>2</sup>Life Sciences Institute, University of Michigan, Ann Arbor, Michigan, USA <sup>3</sup>Department of Medicine, University of California San Diego, San Diego, California, USA <sup>4</sup>Metabolic Signaling, Institute of Bioengineering, School of Life Sciences, Ecole Polytechnique Federale de Lausanne, Switzerland <sup>5</sup>ChemDiv, Inc., San Diego, California, USA <sup>6</sup>Storr Liver Unit, Westmead Millennium Institute, Sydney Medical School, University of Sydney, Australia <sup>7</sup>Howard Hughes Medical Institute, Salk Institute for Biological Studies, La Jolla, California, USA

### Abstract

The systemic expression of the bile acid (BA) sensor farnesoid X receptor (FXR) has led to promising new therapies targeting cholesterol metabolism, triglyceride production, hepatic steatosis and biliary cholestasis. In contrast to systemic therapy, bile acid release during a meal selectively activates intestinal FXR. By mimicking this tissue-selective effect, the gut-restricted FXR agonist fexaramine (Fex) robustly induces enteric fibroblast growth factor 15 (FGF15), leading to alterations in BA composition, but does so without activating FXR target genes in the liver. However, unlike systemic agonism, we find that Fex reduces diet-induced weight gain, body-wide inflammation and hepatic glucose production, while enhancing thermogenesis and browning of white adipose tissue (WAT). These pronounced metabolic improvements suggest tissue-restricted FXR activation as a new approach in the treatment of obesity and metabolic syndrome.

© 2015 Nature America, Inc. All rights reserved.

Reprints and permissions information is available online at <http://www.nature.com/reprints/index.html>.

Correspondence should be addressed to M.D. (downes@salk.edu) or R.M.E. (evans@salk.edu).

**Accession codes.** The RNA-seq data discussed have been deposited in NCBI's Sequence Read Archive and are accessible through accession number [SRP048631](https://www.ncbi.nlm.nih.gov/seq/submit/sra/STP048631).

Note: Any Supplementary Information and Source Data files are available in the [online version of the paper](#).

#### Author Contributions

S.F., J.M.S., M.D. and R.M.E. designed and supervised the research. S.F., J.M.S., S.M.R., E. Yoshihara, O.O., D.L., E. Yu, S.J., S.C. and Y.L. performed research. K.S., A.K., and A.P. performed research and analyzed data. S.F., J.M.S., S.M.R., E. Yoshihara, O.O., D.L., E. Yu, R.T.Y., S.C., C.L., A.R.A., B.S., D.A.B., J.M.O., A.R.S., M.D. and R.M.E. analyzed data. S.F., J.M.S., A.R.A., B.S., D.A.B., C.L., J.M.O., A.R.S., M.D. and R.M.E. wrote the manuscript.

#### COMPETING FINANCIAL INTERESTS

The authors declare competing financial interests: details are available in the [online version of the paper](#).

FXR (encoded by *Nr1h4*) is a ligand-activated transcriptional factor expressed in diverse tissues including the adrenal gland, kidney, stomach, duodenum, jejunum, ileum, colon, gall bladder, liver and macrophages, as well as in white and brown adipose depots<sup>1</sup>. BAs function as endogenous ligands for FXR such that enteric and systemic release of BAs induces FXR-directed changes in gene expression networks<sup>2-8</sup>. The complex role of FXR in metabolic homeostasis is evident in studies on whole body *Nr1h4*<sup>-/-</sup> mice. On a normal chow diet, *Nr1h4*<sup>-/-</sup> mice develop metabolic defects including hyperglycemia and hypercholesterolemia, but, conversely, they exhibit improved glucose homeostasis compared with control mice when challenged with a high-fat diet (HFD)<sup>9,10</sup>. Similar contrary effects are seen with systemic FXR agonists, with beneficial effects observed in chow-fed mice, whereas exacerbated weight gain and glucose intolerance is seen in diet-induced obesity (DIO) mice<sup>11,12</sup>.

In the liver, FXR activation suppresses hepatic BA synthesis, alters BA composition, reduces the BA pool size<sup>13-15</sup> and contributes to liver regeneration<sup>16</sup> as well as glucose, lipid and cholesterol homeostasis<sup>17,18</sup>. Consistent with this, activation of hepatic FXR by the synthetic BA 6 $\alpha$ -ethyl chenodeoxycholic acid is beneficial in the treatment of diabetes, nonalcoholic fatty liver disease and primary biliary cirrhosis<sup>19,20</sup>.

In addition to expression in the liver, FXR is also expressed in the intestine, where it regulates production of the endocrine hormone Fgf15 (FGF19 in humans), which in conjunction with hepatic FXR is thought to control BA synthesis, transport and metabolism<sup>21-23</sup>. Although intestinal FXR activity is also involved in reducing overgrowth of the microbiome during feeding<sup>24,25</sup>, the role of food-activated (prandial) intestinal FXR in body physiology is poorly understood.

In response to a meal, bile acids are secreted into the intestine from the gall bladder and acutely activate intestinal FXR. We thus reasoned that it might be feasible to mimic food activation of intestinal FXR by treating mice with a nonabsorbed synthetic FXR agonist. As we now show, orally delivered Fex<sup>26</sup> is poorly absorbed into the circulation, resulting in intestinally restricted FXR activation. Despite this restricted activation, Fex treatment of DIO mice produces a new, striking metabolic profile that includes reduced weight gain, decreased inflammation, browning of WAT and increased insulin sensitization. The beneficial whole-body efficacy achieved with Fex suggests intestinal FXR therapy as a promising and potentially safer approach to systemic FXR agonism in the treatment of insulin resistance and metabolic syndrome.

## RESULTS

### Orally active Fex shows minimal systemic exposure

We previously reported the development and *in vitro* characterization of Fex as a specific and potent FXR agonist<sup>26</sup>. In exploring the *in vivo* effects, we discovered that due to poor absorption, oral (p.o.) and intraperitoneal (i.p.) drug delivery produced very different effects (Fig. 1a,b). The i.p. Fex treatment (100 mg kg<sup>-1</sup> for 5 d) produced robust induction of the FXR target gene *Nr0b2* (which encodes for SHP, small heterodimer partner) in the liver,

kidney and gut, whereas p.o. administration of Fex produced only intestinal *Nr0b2* induction (Fig. 1c). Consistent with these observations, acute p.o. treatment with Fex induced multiple intestinal FXR target genes including *Fabp6* (encoding IBABP, ileal bile acid binding protein), *Slc51a* (encoding OST- $\alpha$ , organic solute transporter  $\alpha$ ) and *Fgf15*, but failed to activate their expression in either liver or kidney (Fig. 1d and Supplementary Fig. 1). Quantification revealed that drug levels were lower by an order of magnitude after acute p.o. treatment compared with i.p. treatment (Fig. 1a,b), with serum levels of Fex after p.o. administration below the 25 nM half-maximum effective concentration of Fex<sup>26</sup>, in keeping with the lack of target gene activation in kidney and liver.

### Fex counters obesity and metabolic syndrome

To investigate the systemic effects of enteric FXR activation, mice were subjected to 5 weeks of daily Fex treatment by oral gavage (100 mg kg<sup>-1</sup> Fex). Chronically treated chow-fed mice were indistinguishable from vehicle-treated mice in terms of weight gain, basal metabolic activity and glucose tolerance (Supplementary Fig. 2). In contrast, Fex-treated DIO mice (C57BL/6J mice after 14 weeks of a 60% fat diet) showed a dose-dependent reduction in weight gain (Fig. 2a and Supplementary Fig. 3b) with no signs of intestinal toxicity (Supplementary Fig. 4). The reduction in weight gain of Fex-treated mice was largely attributed to reduced overall fat mass, with significant reductions in wet weights of both subcutaneous (inguinal) and visceral (gonadal and mesenteric) adipose depots (Fig. 2b,c). Consistent with reduced adiposity, Fex-treated mice showed significant improvements in their endocrine and metabolic profiles including reduced glucose, insulin, leptin, cholesterol and resistin levels (Fig. 2d and Supplementary Fig. 3a). In addition, serum levels of the inflammatory cytokines tumor necrosis factor- $\alpha$  (Tnf- $\alpha$ ), interleukin (Il)-1 $\alpha$ , Il-1 $\beta$ , Il-17 and mast cell protease-1 (Mcp-1) were markedly decreased (Fig. 2e). Furthermore, Fex treatment induced dose-dependent improvements in glucose tolerance and insulin sensitivity in DIO mice (measured by glucose and insulin tolerance tests; Fig. 2f,g and Supplementary Fig. 3c), but had no effect in normal chow-fed mice (Supplementary Fig. 2d). Notably, these Fex-induced changes in gene expression and improvements in metabolic homeostasis were abrogated in Fex-treated *Nr1h4*<sup>-/-</sup> mice, establishing the FXR dependence of the observed effects (Supplementary Fig. 5).

### Fex enhances energy expenditure in brown adipose tissue

As the differential weight effect was not attributable to a difference in food intake between vehicle and Fex-treated mice (Fig. 3a), we compared the metabolic rates of weight-matched mice. Fex-treated DIO mice had consistently higher oxygen consumption (VO<sub>2</sub>) and exhaled more carbon dioxide (VCO<sub>2</sub>) than vehicle-treated controls (Fig. 3b,c), but displayed similar respiratory exchange ratios, suggesting enhanced use of both sugar and fat (Supplementary Fig. 6). As determined by ambulatory counts, Fex-treated mice were more active than control mice, which may be a reflection of their lower body weights, supporting increased energy expenditure (Fig. 3d).

Consistent with increased energy expenditure, Fex treatment increased the core body temperature of the mice by approximately 1.5 °C (Fig. 3e). In addition, the prominent accumulation of lipid vesicles in brown adipose tissue (BAT) of vehicle-treated DIO mice

was markedly reduced in Fex-treated mice (Fig. 3f). Gene expression analysis confirmed the induction of *Esrrg* (encoding estrogen receptor related- $\gamma$  (ERR- $\gamma$ )), *Ppargc1a* (encoding PGC-1 $\alpha$ , peroxisome proliferator-activated receptor  $\gamma$  coactivator 1 $\alpha$ ) and *Ppargc1b* (encoding PGC-1 $\beta$ ), as well as a number of their target genes involved in thermogenesis, mitochondrial biogenesis and fatty acid oxidation in BAT (Fig. 3g). Moreover, Fex treatment increased the phosphorylation level of p38 (Fig. 3h and Supplementary Fig. 7a), which has been shown to stabilize PGC-1 $\alpha$ , a key coactivator of the thermogenic transcriptional program in BAT<sup>27</sup>. A comparison of the transcriptional changes induced by Fex in inguinal, gonadal and brown adipose depots revealed coordinated changes that selectively enhance oxidative phosphorylation activity in BAT, suggesting that BAT is a key contributor to the increased energy expenditure and thermogenesis (Supplementary Fig. 7b). Consistent with this suggestion, KEGG pathway analysis of Fex-induced transcriptional changes in BAT identified oxidative phosphorylation and the chemokine/cytokine signaling pathway as significantly changed (Supplementary Fig. 7c,d), whereas increased protein kinase A activity was also seen in Fex-treated mice (Supplementary Fig. 7e). Furthermore, serum lactate levels were significantly reduced in Fex-treated DIO mice, suggesting that body-wide energy metabolism is shifted toward a more oxidative state (Supplementary Fig. 7f). Thus, the marked reductions in lipids, increased protein kinase A activity and p38 phosphorylation, as well as increased core body temperature, indicate a coordinated activation of thermogenesis in BAT in Fex-treated DIO mice.

### Fex induces Fgf15 and alters BA composition

RNA-seq of intestinal tissues was used to explore the mechanisms through which Fex might contribute to systemic changes in energy expenditure and metabolic rate. KEGG pathway analysis revealed induction of multiple metabolic pathways including peroxisome proliferator-activated receptor and adipocytokine signaling in both ileum and colon (Supplementary Fig. 8a). Overlap of Fex-induced expression changes with previously identified intestinal FXR binding sites<sup>28</sup> identified a subset of genes as potential direct FXR targets (Fig. 4a). Within this subset, *Fgf15* was found to be markedly upregulated by Fex. In addition to established FXR target genes such as *Lpl*, other genes potentially regulated by FXR were identified, including the circadian regulator *Per1* (Fig. 4a).

As it encodes an intestinal endocrine hormone, *Fgf15* induction is of particular interest because Fgf15 is known to activate the thermogenic program in BAT<sup>29</sup>. Fgf15 also negatively regulates BA synthesis through suppression of hepatic *Cyp7a1*, which encodes the rate-limiting enzyme for BA synthesis<sup>22,23,30</sup>. As expected, endogenous serum Fgf15 levels were too low to be detected in vehicle-treated mice. However, prolonged intestinal FXR activation by Fex treatment resulted in a sustained increase in Fgf15 production. We were able to measure an increase in circulating Fgf15 that accompanied the increase in mRNA expression in ileum (Fig. 4b,c). Consistent with this increase in serum Fgf15, hepatic *Cyp7a1* was significantly repressed at both the mRNA and protein level after chronic Fex treatment, whereas the expression of *Cyp8b1* and *Cyp27a1* were not significantly affected. However, the expression of *Cyp7b1*, encoding a key enzyme in the alternate (acidic) pathway of BA synthesis, which bypasses *Cyp7a1*, was increased (Fig. 4d and Supplementary Fig. 8b). Notably, expression of the well-established hepatic FXR target

genes *Nr0b2* and *Abcb11* (encoding Bsep, bile salt export pump) was not altered, further demonstrating the absence of liver FXR activation after chronic Fex treatment (Fig. 4d) and implying that other pathways, such as Fgf15, mediate changes in hepatic gene expression.

Despite the apparent absence of hepatic FXR activation, Fex treatment produced striking changes in the composition of the BA pool. In addition to reducing the size of the BA pool, Fex treatment changed the relative proportions of circulating BAs, most notably decreasing the fraction of taurocholic acid and increasing the fraction of the secondary BA, lithocholic acid (Fig. 4e,f and Supplementary Table 1). These changes are consistent with increased intestinal FXR activation, including the effects of increased circulating Fgf15 on BA synthesis in the liver. Indeed, decreased serum taurocholic acid has been previously reported in mice expressing a constitutively activated FXR transgene in intestine, as well as after injection of FGF19, the human analog of Fgf15 (ref. 31). Furthermore, changes in BA synthesis away from cholic acid toward chenodeoxycholic acid and its derivatives, including lithocholic acid, were observed upon FGF19 treatment<sup>31</sup>, consistent with a reduction in hepatic *Cyp7a1* and an increase in *Cyp7b1* expression.

FXR activation has been reported to enhance expression of genes involved in mucosal defense and intestinal barrier function<sup>25,32</sup>. Consistent with these reports, mice showed reduced intestinal permeability, as measured by fluorescein isothiocyanate (FITC)-dextran leakage into the serum, and increased expression of mucosal defense genes *Ocln* (encoding occludin) and *Muc2* after chronic treatment with Fex (Fig. 4g,h).

Although Fex does not activate the G protein-coupled BA receptor Tgr5 (encoded by *Gpbar1*) (Supplementary Fig. 9), the pronounced changes in BAs suggested that this pathway might contribute to the observed physiologic effects. Notably, treatment of mice fed an HFD with the intestinally restricted Tgr5 agonist L7550379 did not induce metabolic changes, whereas treatment with the systemic Tgr5 agonist RO5527239 improved glucose homeostasis, as measured by glucose tolerance test and insulin secretion (Supplementary Fig. 10). These findings suggested that Tgr5 activation outside of the intestine may contribute to the beneficial effects of Fex treatment<sup>33</sup> (Supplementary Fig. 10b,d-f). To address this possibility, *Gpbar1*<sup>-/-</sup> mice fed an HFD were chronically treated with Fex (100 mg kg<sup>-1</sup> d<sup>-1</sup> p.o. for 5 weeks). As seen in wild-type mice, Fex treatment induced multiple FXR target genes in the ileum of *Gpbar1*<sup>-/-</sup> mice including Fgf15, resulting in lowered serum BA levels (Supplementary Fig. 11a,b). In this *Gpbar1*<sup>-/-</sup> background, Fex treatment induced moderate improvements in fasting glucose levels and glucose tolerance (Supplementary Fig. 11c). In addition, somewhat blunted increases in core body temperature and metabolic rate, correlating with the induction of thermogenic genes in BAT, were observed (Supplementary Fig. 11d,e), suggesting that these effects do not require Tgr5 activation. In contrast to wild-type mice, no significant changes in weight gain or insulin sensitivity were observed in Fex-treated *Gpbar1*<sup>-/-</sup> mice, and altered gene expression patterns were seen in the liver and muscle, indicating involvement of the Tgr5 pathway (Supplementary Fig. 11f-j). In particular, the antilipogenic effects of Fex in the liver seem to require Tgr5 activation, as key hepatic lipogenic genes and liver triglyceride content were not affected by Fex treatment (Supplementary Fig. 11h,i).

## Fex induces browning of WAT

During obesity, adipose tissue expands by hyperplastic and/or hypertrophic growth, is chronically inflamed and produces inflammatory cytokines that ultimately contribute to systemic metabolic dysregulation. After chronic treatment of DIO mice with Fex, the cross-sectional area of adipocytes in visceral depots, including gonadal and mesenteric adipocytes, was markedly reduced compared to vehicle (Fig. 5a). An investigation of signaling pathways implicated in diet-induced inflammation identified reduced levels of IKK- $\epsilon$  and TANK-binding kinase 1 in Fex-treated DIO mice (Fig. 5b and Supplementary Fig. 12a). These noncanonical I $\kappa$ B kinases were recently shown to have crucial roles in energy expenditure as a consequence of adipose tissue inflammation upon diet-induced obesity<sup>34</sup>. In addition, activation of the mammalian target of rapamycin complex 1 (mTORC1) pathway, a key lipogenic pathway activated by an HFD, was reduced in Fex-treated gonadal WAT, as evidenced by reduced S6 kinase phosphorylation (Fig. 5b). Consistent with reduced adiposity, gene expression of the inflammatory cytokines was reduced in visceral and brown adipose depots of Fex-treated mice compared to vehicle (Fig. 5c and Supplementary Fig. 12b).

Brown adipose-driven adaptive thermogenesis is fueled by mitochondrial oxidation of free fatty acids (FFAs) released from triglyceride stores into the circulation, predominantly by the action of hormone-sensitive lipase (Hsl). Low levels of Hsl phosphorylation were seen in visceral and subcutaneous adipose depots from control mice, as expected due to desensitization of the  $\beta$ -adrenergic pathway in WAT during obesity<sup>35,36</sup>. In contrast, when compared with vehicle treatment, a pronounced increase in Hsl phosphorylation and FFA levels (Fig. 5d,f), accompanied by increased serum catecholamine levels and  $\beta$ 3-adrenergic receptor expression (Fig. 5c,e), was observed after chronic treatment with Fex. As  $\beta$ -adrenergic receptor activation has been shown to induce brown fat-like cells in inguinal adipose tissue, and these cells have been associated with resistance to diet-induced obesity and improved glucose metabolism<sup>37–40</sup>, we examined *Ucp1* expression in inguinal adipose tissue. Immunohistochemistry revealed a substantial increase in the abundance of multilocular, *Ucp1*-expressing adipocytes in Fex-treated animals (Fig. 5g). Furthermore, Fex treatment increased the expression of brown fat-like signature genes and increased respiratory capacity in the stromal vascular fraction from inguinal adipose tissue (Supplementary Fig. 13a,b). These results indicate that Fex, unlike systemic FXR ligands, induces a distinct coordinated metabolic response that enhances  $\beta$ -adrenergic signaling to promote lipolysis and mobilizes fatty acids for oxidation in BAT and the ‘browning’ of cells in WAT.

## Fex improves insulin responsiveness

To probe the mechanism through which chronic Fex treatment improved glucose homeostasis, we carried out hyperinsulinemic-euglycemic clamp studies. No differences in basal hepatic glucose production (HGP), glucose disposal rate (GDR), insulin-stimulated GDR, FFA suppression and fasting insulin levels were observed between weight-matched cohorts (generated by treating initially heavier mice (2–3 g) with Fex; Fig. 6a–c and Supplementary Fig. 14). However, Fex-treated mice displayed a marked increase in insulin-mediated suppression of HGP compared with control DIO mice (Fig. 6d). Thus, while the

attenuated weight gain likely contributes to improved glucose clearance in Fex-treated mice, this improvement in hepatic glucose suppression indicates enhanced liver insulin sensitivity after Fex treatment.

Liver insulin resistance has been linked to obesity-induced hepatic steatosis<sup>41</sup>. Histological examination of liver tissue from Fex-treated DIO mice revealed a reduction in lipid droplets compared with controls, indicating amelioration of hepatic steatosis (Fig. 6e). Consistent with this histology, a marked decrease in hepatic triglycerides and reduced hepatic expression of gluconeogenic and lipogenic genes were seen after chronic Fex treatment (Fig. 6f,g). Furthermore, decreased serum alanine aminotransferase (ALT) levels were measured in Fex-treated mice, indicative of reduced liver damage induced by an HFD (Fig. 6h). Thus, in DIO mice, Fex promotes hepatic insulin sensitization, reduced steatosis, improved metabolic markers, decreased ALT and enhanced BAT activity.

## DISCUSSION

Here we show that the gut-biased FXR agonist Fex has substantial metabolic benefits in a mouse model of obesity. Fex protects against diet-induced weight gain by promoting the expression of genes involved in thermogenesis, mitochondrial biogenesis and fatty acid oxidation. Linked to the unexpected browning of white adipose, Fex lowers inflammatory cytokine levels while upregulating  $\beta$ -adrenergic signaling. These changes seem to be mediated in part by a change in BA levels and composition. In addition, intestinal-specific FXR activation corrected numerous obesity-related defects, enhanced glucose tolerance and lowered hepatic glucose production. Notably, these physiologic changes are dependent on FXR expression and result in hepatic insulin sensitization and BAT activation, properties not formerly associated with this class of drug.

How might this be achieved? The initial event triggering systemic metabolic activation is probably coordinated by Fgf15, a key regulator of energy expenditure reported to increase metabolic rate and improve glucose and lipid homeostasis without significant changes in food intake<sup>29,42</sup>. The absence of a change in food intake is notable, as failure of appetite control is a major reason for weight gain<sup>43</sup>. Thus, systemic increases in energy expenditure, as seen in Fex-treated mice, may offer a viable alternative for obesity treatments. However, this explanation alone is not sufficient, as systemic FXR agonists, while robustly inducing Fgf15, do not display many of the benefits of gut-biased FXR activation.

One major difference between gut-biased and systemic FXR activation is the effect on serum BAs, which for Fex includes a marked change in the relative composition of circulating BAs. A reduction in hepatic *Cyp7a1* accompanied by an increase in *Cyp7b1* expression shifts BA synthesis away from cholic acid toward chenodeoxycholic acid derivatives, most notably lithocholic acid. While the absolute amount of lithocholic acid did not change following treatment with Fex, the relative amount increased dramatically. Lithocholic acid is a hydrophobic secondary BA and the most potent endogenous ligand for the G protein-coupled BA receptor Tgr5 (ref. 33). Notably, Fex treatment induces metabolic changes similar to those observed with systemic administration of a synthetic Tgr5 agonist<sup>33</sup>. Also, induction of *Dio2*, a downstream target of Tgr5 (ref. 44), in BAT with oral

Fex implicates this pathway in the increased energy expenditure. Indeed, the metabolic improvements attributed to Fex treatment were tempered in *Gpbar1*<sup>-/-</sup> mice, suggesting that Tgr5 activation is important in mediating selective aspects of Fex signaling. Furthermore, the coordinated browning of the WAT depot provides an independent yet complementary contribution to increased thermogenic capacity<sup>37-40</sup>.

These studies uncover a new therapeutic avenue to manipulate energy expenditure without appetite changes through intestinally biased activation of the nuclear receptor FXR. Although contrary indications supporting roles for FXR antagonists have been reported<sup>21,24</sup>, the integral role of FXR in gut homeostasis provides therapeutic advantages in gene activation. Gut-restricted drugs such as Fex inherently offer improved safety profiles, achieving systemic efficacy while avoiding systemic toxicity. In support of the remarkable metabolic improvements achieved via oral Fex treatment, intestinal FXR has been recently identified as a molecular target of vertical sleeve gastrectomy<sup>45</sup>, suggesting that Fex may offer a nonsurgical alternative for the control of metabolic disease.

## ONLINE METHODS

### Animals and animal care

We fed wild-type male C57BL/6J mice an HFD consisting of 60% of calories from fat starting at 6 weeks of age for 14 weeks (Jackson, catalog no. 380050). After then, each mouse consumed on average 50 mg or 100 mg per kg body weight Fex (in corn oil) per day by oral gavage for 5 weeks on HFD. *Nr1h4*<sup>-/-</sup> mice were purchased from Jackson Laboratory. *Gpbar1*<sup>-/-</sup> mice (provided by K.S.) were fed an HFD (Research diet D12492) from 8 weeks of age. The sample sizes for all animal studies are indicated in each figure legend. All mice were housed in a specific pathogen-free facility with a 12-h light, 12-h dark cycle and given free access to food and water. All *in vivo* data were retrieved from 3 independent experimental animal cohorts. Core body temperature was measured with a clinical rectal thermometer (Thermalert model TH-5; Physitemp). Total cholesterol, TG, insulin, FFAs, leptin, ALT and adiponectin were determined using enzymatic reactions. For hepatic lipid analysis, the lipid was extracted according to the Folch method and resuspended in PBS containing 5% Triton X-100. For GTTs, overnight-fasted mice received 2 g of glucose per kg of body weight via i.p. injection. Human insulin (Humilin, Eli Lilly) was used for insulin tolerance test. Tail blood was drawn at indicated time intervals, and blood glucose level was measured with a One Touch Ultra glucometer (LifeScan). Body composition was measured with Echo MRI-100 body composition analyzer (Echo Medical Systems). For histology, 5- $\mu$ m sections were stained with H&E. All mice were randomly assigned to experimental groups for further analysis. No samples were excluded from the analysis. All protocols for mouse experiments were approved by the Institutional Animal Care and Use Committee of The Salk Institute.

### *In vivo* metabolic phenotype analysis

Real-time metabolic analyses were conducted in a Comprehensive Lab Animal Monitoring System (Columbus Instruments). CO<sub>2</sub> production, O<sub>2</sub> consumption, RQ (relative rates of

carbohydrate versus fat oxidation) and ambulatory counts were determined for 6 consecutive days and nights, with at least 24 h for adaptation before data recording.

### Extracellular oxygen consumption rate assay

Briefly, stromal vascular fraction (SVF) was isolated from inguinal adipose tissues using collagenase type I (Sigma). Cells were seeded in XF 96-well cell culture microplates (Seahorse Bioscience) at  $5.0 \times 10^4$  cells per well in 150  $\mu$ l of growth medium and then incubated at 37 °C/5% CO<sub>2</sub> for 24 h. A Seahorse Bioscience instrument model XF96 was used to measure the rate of change of dissolved oxygen in the media surrounding the cells. All procedures followed manufacturer's instructions. Oxygen consumption rates were normalized by the number of cells to reflect the metabolic activities of the cells.

### Cytokine analysis

Serum levels of mouse cytokines were analyzed by Luminex Bio-Plex system. The mouse cytokine 23-multiplex assay was carried out according to the manufacturer's instructions (Bio-Rad).

### Serum BA composition analysis

Serum (100  $\mu$ l) was protein precipitated with 300  $\mu$ l of cold acetonitrile containing deuterated cholic acid as an internal standard, vortexed and centrifuged at 10,000 rpm for 10 min at 4 °C.

Supernatant (300  $\mu$ l) was evaporated under nitrogen and reconstituted in assay mobile phase. BA separation was achieved on a C18 column (Waters X-Terra MS 3.5  $\mu$ m, 2.1  $\times$  150 mm maintained at 40 °C) using a binary solvent gradient (solvent A, 10% ACN in 10  $\mu$ M ammonium acetate, pH 4.5; solvent B, 90% ACN in 10  $\mu$ M ammonium acetate, pH 4.5) or a tertiary gradient (HDCA, UCDA, and glycol and tauro conjugates required solvent C: 90% MeOH in 10 mM ammonium acetate, pH 4.5), and were detected as negative ions after electrospray ionization in an Agilent series 6120 quadrupole mass detector.

### Gene expression analysis

Total RNA was isolated from mouse tissues using TRIzol reagent (Invitrogen) as per the manufacturer's instructions. mRNA levels were quantified by quantitative PCR with SYBR Green (Invitrogen). cDNA was synthesized from 1  $\mu$ g of DNase-treated total RNA using SuperScript II reverse transcriptase (Invitrogen). Samples were run in technical triplicates and relative mRNA levels were calculated by using the standard curve methodology and normalized against 36B4 mRNA levels in the same samples.

### RNA-seq library generation

Total RNA was isolated from mouse tissues treated with RNAlater using the RNA mini kit (Qiagen) and treated with DNaseI (Qiagen) for 30 min at 22 °C. Sequencing libraries were prepared from 100–500 ng of total RNA using the TruSeq RNA sample preparation kit v2 (Illumina) according to the manufacturer's protocol. Briefly, mRNA was purified, fragmented and used for first- and second-strand cDNA synthesis followed by adenylation of 3' ends. Samples were ligated to unique adaptors and subjected to PCR amplification.

Libraries were then validated using the 2100 BioAnalyzer (Agilent), normalized and pooled for sequencing. RNA-seq libraries prepared from two biological replicates for each experimental condition were sequenced on the Illumina HiSeq 2000 using barcoded multiplexing and a 100-bp read length.

### High-throughput sequencing and analysis

Image analysis and base calling were done with Illumina CASAVA-1.8.2. This yielded a median of 29.9M usable reads per sample. Short read sequences were mapped to a UCSC mm9 reference sequence using the RNA-seq aligner STAR<sup>46</sup>. Known splice junctions from mm9 were supplied to the aligner and *de novo* junction discovery was also permitted. Differential gene expression analysis, statistical testing and annotation were performed using Cuffdiff 2 (ref. 47). Transcript expression was calculated as gene-level relative abundance in fragments per kilobase of exon model per million mapped fragments and employed correction for transcript abundance bias<sup>48</sup>. RNA-seq results for genes of interest were also explored visually using the UCSC Genome Browser.

### Western blot analysis

We homogenized tissues in lysis buffer (50 mM Tris, pH 7.5, 5 mM EDTA, 250 mM sucrose, 1% NP-40, 2 mM dithiothreitol (DTT), 1 mM sodium vanadate, 100 mM NaF, 10 mM Na<sub>4</sub>P<sub>2</sub>O<sub>7</sub> and freshly added protease inhibitor tablet) and then incubated them for 1 h at 4 °C. We centrifuged crude lysates at 14,000g for 15 min twice and determined the protein concentration using Bio-Rad protein assay reagent. Samples were diluted in SDS sample buffer. Bound proteins were resolved by SDS-PAGE and transferred to nitrocellulose membranes (Bio-Rad). Individual proteins were detected with the specific antibodies and visualized on film using horseradish peroxidase–conjugated secondary antibodies (Bio-Rad) and Western Lightning enhanced chemiluminescence (PerkinElmer Life Sciences). Alternatively, infrared fluorescent secondary antibodies were used for detection and quantification of specific protein on the Odyssey CLx imager (LI-COR). Antibodies to IKK $\epsilon$  (cat. no. 2690), TBK1 (cat. no. 3013), pTBK1 (Ser172; cat. no. 5483), S6K (cat. no. 2708, diluted 1:250), pS6K (Thr389; cat. no. 9205), HSL (cat. no. 4107) and pHSL (Ser563; cat. no. 4139 or Ser660; cat. no. 4126) were purchased from Sigma-Aldrich and used at dilutions specified by the manufacturer.

### Fgf15 ELISA

Fgf15 concentrations were measured from serum and ileal tissue extracts using a commercial ELISA kit (Uscn Life Science, kit no. SEL154Mu). ELISA was done according to the manufacturer's protocol. Antibody specificity was confirmed previously<sup>49</sup>.

### Hyperinsulinemic-euglycemic clamp

Diet-induced obese C57BL/6J mice fed a 60% HFD for 12 weeks were obtained from Jackson Laboratory. Mice were gavaged with 100 mg/kg Fex or corn oil vehicle daily for 3 weeks before hyperinsulinemic-euglycemic clamp studies. Clamp studies were performed as described<sup>50</sup>. Briefly, dual catheters (cat. no. MRE025, Braintree Scientific) were implanted in the right jugular vein, tunneled subcutaneously and exteriorized at the back of the neck.

Mice were allowed to recover for 4–5 d before the clamp procedure. After 6 h of fasting, mice were placed in a Lucite restrainer (Braintree Scientific) and blood glucose was measured via tail nick. The experiment began with a constant infusion (5 Ci/h) of D-[3-<sup>3</sup>H] glucose (PerkinElmer NEN Radiochemicals) via the jugular vein cannulae. After 90 min of tracer equilibration and basal blood sampling at –10 and 0 min, insulin (8 mU/kg/min, Novo Nordisk) plus tracer (5 Ci/h) and glucose (50% dextrose at variable rate, Abbott) infusions were initiated via the jugular vein cannulae simultaneously, with glucose infusion rate adjusted to reach a steady state blood glucose concentration (~120 min). Blood samples were collected via tail vein at –10, 0 (basal), 110 and 120 (steady-state) min to determine glucose-specific activity, and insulin and FFA levels. Steady-state conditions (120 mg/dl ± 10 mg/dl) were confirmed at the end of the clamp by ensuring that glucose infusion rate and plasma glucose levels maintained constant for 30 min. Tracer-determined HGP and GDR were calculated at the basal state and during the steady-state portions of the clamp by using the Steele equation for steady-state conditions. At steady state, the rate of glucose disappearance (total GDR) is equal to the sum of the rate of endogenous glucose production (that is, HGP) plus the exogenous (cold) GIR. The IS-GDR is equal to the total GDR minus the basal glucose turnover rate.

### Statistical analysis

Appropriate statistical analyses were applied, assuming a normal sample distribution, as specified in the figure legends. Statistics were done using Student's *t*-test. Values were presented as mean ± sd. No samples were excluded from the statistical analyses as investigators were not blinded in the studies. Variances for each group data were calculated and used for Student's *t*-test. Animal cohort sizes were determined on the basis of similar previous studies.

### Supplementary Material

Refer to Web version on PubMed Central for supplementary material.

### Acknowledgments

We thank H. Juguilon, L. Chong, Y. Yin, J. Alvarez, Y. Dai, S. Kaufman and B. Collins for technical assistance, and L. Ong and C. Brondos for administrative assistance. R.M.E. is an Investigator of the Howard Hughes Medical Institute (HHMI) at the Salk Institute and March of Dimes Chair in Molecular and Developmental Biology, and is supported by National Institutes of Health (NIH) grants (DK057978, DK090962, HL088093, HL105278 and ES010337), the Glenn Foundation for Medical Research, the Leona M. and Harry B. Helmsley Charitable Trust, Ipsen/Biomeasure, California Institute for Regenerative Medicine and The Ellison Medical Foundation. C.L. and M.D. are funded by grants from the National Health and Medical Research Council of Australia Project Grants 512354, 632886 and 1043199; J.M.O. is supported by NIH grants (DK033651, DK074868, T32-DK007494, DK063491 and P01-DK054441-14A1) and by the Eunice Kennedy Shriver National Institute of Child Health and Human Development/NIH through cooperative agreement of U54-HD-012303-25 as part of the specialized Cooperative Centers Program in Reproduction and Infertility Research; A.R.S. is supported by NIH grants (DK60597 and DK61618). R.M.E., J.M.O., A.R.S. and D.A.B. are supported by NIH grant R24DK090962.

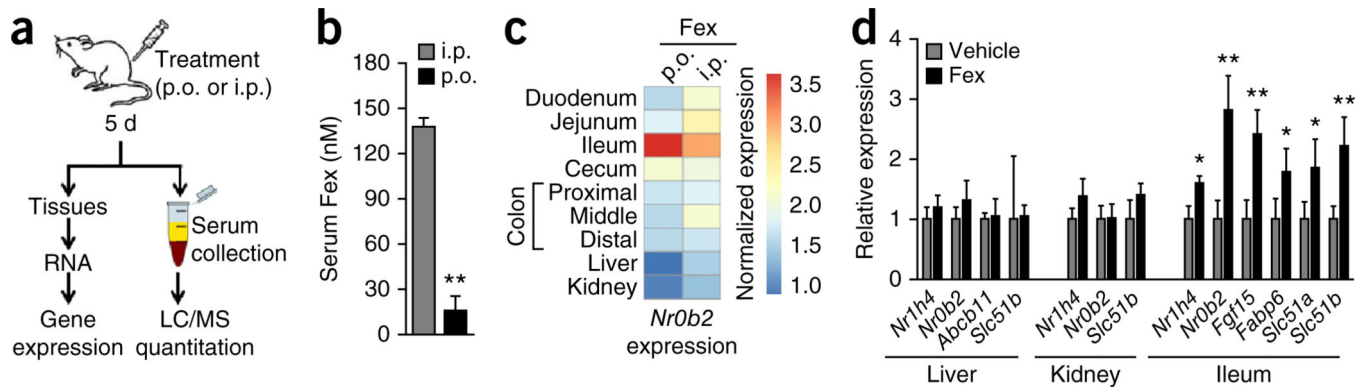
### References

1. Forman BM, et al. Identification of a nuclear receptor that is activated by farnesol metabolites. *Cell*. 1995; 81:687–693. [PubMed: 7774010]

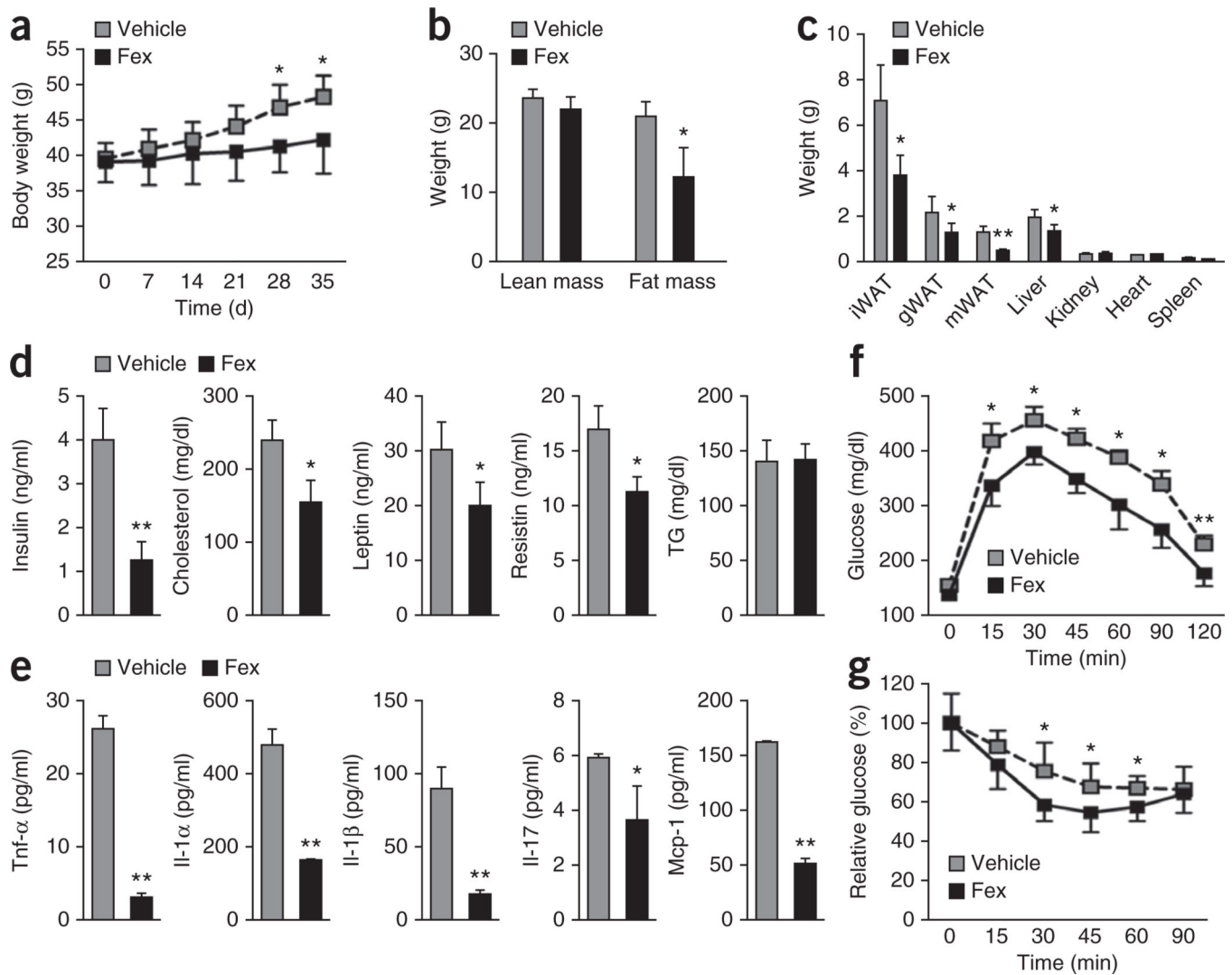
2. Lee FY, Lee H, Hubbert ML, Edwards PA, Zhang Y. FXR, a multipurpose nuclear receptor. *Trends Biochem. Sci.* 2006; 31:572–580. [PubMed: 16908160]
3. Repa JJ, et al. Regulation of absorption and ABC1-mediated efflux of cholesterol by RXR heterodimers. *Science.* 2000; 289:1524–1529. [PubMed: 10968783]
4. Zollner G, et al. Role of nuclear bile acid receptor, FXR, in adaptive ABC transporter regulation by cholic and ursodeoxycholic acid in mouse liver, kidney and intestine. *J. Hepatol.* 2003; 39:480–488. [PubMed: 12971955]
5. Fang S, et al. The p300 acetylase is critical for ligand-activated farnesoid X receptor (FXR) induction of SHP. *J. Biol. Chem.* 2008; 283:35086–35095. [PubMed: 18842595]
6. Kemper JK, et al. FXR acetylation is normally dynamically regulated by p300 and SIRT1 but constitutively elevated in metabolic disease states. *Cell Metab.* 2009; 10:392–404. [PubMed: 19883617]
7. Makishima M, et al. Identification of a nuclear receptor for bile acids. *Science.* 1999; 284:1362–1365. [PubMed: 10334992]
8. Stedman C, et al. Benefit of farnesoid X receptor inhibition in obstructive cholestasis. *Proc. Natl. Acad. Sci. USA.* 2006; 103:11323–11328. [PubMed: 16844773]
9. Sinal CJ, et al. Targeted disruption of the nuclear receptor FXR/BAR impairs bile acid and lipid homeostasis. *Cell.* 2000; 102:731–744. [PubMed: 11030617]
10. Prawitt J, et al. Farnesoid X receptor deficiency improves glucose homeostasis in mouse models of obesity. *Diabetes.* 2011; 60:1861–1871. [PubMed: 21593203]
11. Zhang Y, et al. Activation of the nuclear receptor FXR improves hyperglycemia and hyperlipidemia in diabetic mice. *Proc. Natl. Acad. Sci. USA.* 2006; 103:1006–1011. [PubMed: 16410358]
12. Watanabe M, et al. Lowering bile acid pool size with a synthetic farnesoid X receptor (FXR) agonist induces obesity and diabetes through reduced energy expenditure. *J. Biol. Chem.* 2011; 286:26913–26920. [PubMed: 21632533]
13. Wang L, et al. Redundant pathways for negative feedback regulation of bile acid production. *Dev. Cell.* 2002; 2:721–731. [PubMed: 12062085]
14. Fang S, et al. Coordinated recruitment of histone methyltransferase G9a and other chromatin-modifying enzymes in SHP-mediated regulation of hepatic bile acid metabolism. *Mol. Cell. Biol.* 2007; 27:1407–1424. [PubMed: 17145766]
15. Lu TT, et al. Molecular basis for feedback regulation of bile acid synthesis by nuclear receptors. *Mol. Cell.* 2000; 6:507–515. [PubMed: 11030331]
16. Huang W, et al. Nuclear receptor-dependent bile acid signaling is required for normal liver regeneration. *Science.* 2006; 312:233–236. [PubMed: 16614213]
17. Zhang Y, Castellani LW, Sinal CJ, Gonzalez FJ, Edwards PA. Peroxisome proliferator-activated receptor- $\gamma$  coactivator 1 $\alpha$  (PGC-1 $\alpha$ ) regulates triglyceride metabolism by activation of the nuclear receptor FXR. *Genes Dev.* 2004; 18:157–169. [PubMed: 14729567]
18. Ma K, Saha PK, Chan L, Moore DD. Farnesoid X receptor is essential for normal glucose homeostasis. *J. Clin. Invest.* 2006; 116:1102–1109. [PubMed: 16557297]
19. Stanimirov B, Stankov K, Mikov M. Pleiotropic functions of bile acids mediated by the farnesoid X receptor. *Acta Gastroenterol. Belg.* 2012; 75:389–398. [PubMed: 23402081]
20. Mudaliar S, et al. Efficacy and safety of the farnesoid X receptor agonist obeticholic acid in patients with type 2 diabetes and nonalcoholic fatty liver disease. *Gastroenterology.* 2013; 145:574–582. e571. [PubMed: 23727264]
21. Kim I, et al. Differential regulation of bile acid homeostasis by the farnesoid X receptor in liver and intestine. *J. Lipid Res.* 2007; 48:2664–2672. [PubMed: 17720959]
22. Song KH, Li T, Owsley E, Strom S, Chiang JY. Bile acids activate fibroblast growth factor 19 signaling in human hepatocytes to inhibit cholesterol 7 $\alpha$ -hydroxylase gene expression. *Hepatology.* 2009; 49:297–305. [PubMed: 19085950]
23. Inagaki T, et al. Fibroblast growth factor 15 functions as an enterohepatic signal to regulate bile acid homeostasis. *Cell Metab.* 2005; 2:217–225. [PubMed: 16213224]

24. Li F, et al. Microbiome remodelling leads to inhibition of intestinal farnesoid X receptor signalling and decreased obesity. *Nat. Commun.* 2013; 4:2384. [PubMed: 24064762]
25. Inagaki T, et al. Regulation of antibacterial defense in the small intestine by the nuclear bile acid receptor. *Proc. Natl. Acad. Sci. USA.* 2006; 103:3920–3925. [PubMed: 16473946]
26. Downes M, et al. A chemical, genetic, and structural analysis of the nuclear bile acid receptor FXR. *Mol. Cell.* 2003; 11:1079–1092. [PubMed: 12718892]
27. Cao W, et al. p38 mitogen-activated protein kinase is the central regulator of cyclic AMP-dependent transcription of the brown fat uncoupling protein 1 gene. *Mol. Cell. Biol.* 2004; 24:3057–3067. [PubMed: 15024092]
28. Thomas AM, et al. Genome-wide tissue-specific farnesoid X receptor binding in mouse liver and intestine. *Hepatology.* 2010; 51:1410–1419. [PubMed: 20091679]
29. Fu L, et al. Fibroblast growth factor 19 increases metabolic rate and reverses dietary and leptin-deficient diabetes. *Endocrinology.* 2004; 145:2594–2603. [PubMed: 14976145]
30. Stroeve JH, et al. Intestinal FXR-mediated FGF15 production contributes to diurnal control of hepatic bile acid synthesis in mice. *Lab. Invest.* 2010; 90:1457–1467. [PubMed: 20531290]
31. Wu AL, et al. FGF19 regulates cell proliferation, glucose and bile acid metabolism via FGFR4-dependent and independent pathways. *PLoS ONE.* 2011; 6:e17868. [PubMed: 21437243]
32. Gadaleta RM, et al. Farnesoid X receptor activation inhibits inflammation and preserves the intestinal barrier in inflammatory bowel disease. *Gut.* 2011; 60:463–472. [PubMed: 21242261]
33. Ullmer C, et al. Systemic bile acid sensing by G protein-coupled bile acid receptor 1 (GPBAR1) promotes PYY and GLP-1 release. *Br. J. Pharmacol.* 2013; 169:671–684. [PubMed: 23488746]
34. Reilly SM, et al. An inhibitor of the protein kinases TBK1 and IKK-varepsilon improves obesity-related metabolic dysfunctions in mice. *Nat. Med.* 2013; 19:313–321. [PubMed: 23396211]
35. Carmen GY, Victor SM. Signalling mechanisms regulating lipolysis. *Cell. Signal.* 2006; 18:401–408. [PubMed: 16182514]
36. Song Y, et al. CRTC3 links catecholamine signalling to energy balance. *Nature.* 2010; 468:933–939. [PubMed: 21164481]
37. Tsukiyama-Kohara K, et al. Adipose tissue reduction in mice lacking the translational inhibitor 4E-BP1. *Nat. Med.* 2001; 7:1128–1132. [PubMed: 11590436]
38. Fisher FM, et al. FGF21 regulates PGC-1 $\alpha$  and browning of white adipose tissues in adaptive thermogenesis. *Genes Dev.* 2012; 26:271–281. [PubMed: 22302939]
39. Hansen JB, et al. Retinoblastoma protein functions as a molecular switch determining white versus brown adipocyte differentiation. *Proc. Natl. Acad. Sci. USA.* 2004; 101:4112–4117. [PubMed: 15024128]
40. Wang H, et al. Liver X receptor  $\alpha$  is a transcriptional repressor of the uncoupling protein 1 gene and the brown fat phenotype. *Mol. Cell. Biol.* 2008; 28:2187–2200. [PubMed: 18195045]
41. Cohen JC, Horton JD, Hobbs HH. Human fatty liver disease: old questions and new insights. *Science.* 2011; 332:1519–1523. [PubMed: 21700865]
42. Bhatnagar S, Damron HA, Hillgartner FB. Fibroblast growth factor-19, a novel factor that inhibits hepatic fatty acid synthesis. *J. Biol. Chem.* 2009; 284:10023–10033. [PubMed: 19233843]
43. Foster-Schubert KE, Cummings DE. Emerging therapeutic strategies for obesity. *Endocr. Rev.* 2006; 27:779–793. [PubMed: 17122357]
44. Watanabe M, et al. Bile acids induce energy expenditure by promoting intracellular thyroid hormone activation. *Nature.* 2006; 439:484–489. [PubMed: 16400329]
45. Ryan KK, et al. FXR is a molecular target for the effects of vertical sleeve gastrectomy. *Nature.* 2014; 509:183–188. [PubMed: 24670636]
46. Dobin A, et al. STAR: ultrafast universal RNA-seq aligner. *Bioinformatics.* 2013; 29:15–21. [PubMed: 23104886]
47. Trapnell C, et al. Differential analysis of gene regulation at transcript resolution with RNA-seq. *Nat. Biotechnol.* 2013; 31:46–53. [PubMed: 23222703]
48. Roberts A, Pimentel H, Trapnell C, Pachter L. Identification of novel transcripts in annotated genomes using RNA-seq. *Bioinformatics.* 2011; 27:2325–2329. [PubMed: 21697122]

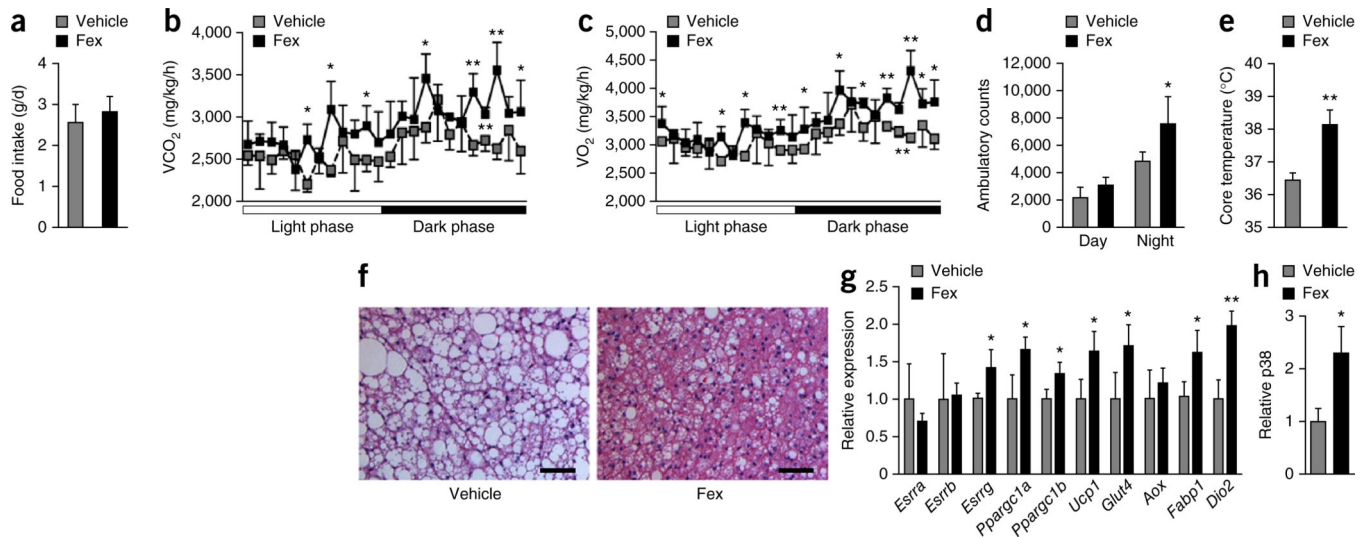
49. Vergnes L, Lee JM, Chin RG, Auwerx J, Reue K. Diet1 functions in the FGF15/19 enterohepatic signaling axis to modulate bile acid and lipid levels. *Cell Metab.* 2013; 17:916–928. [PubMed: 23747249]
50. Osborn O, et al. G protein–coupled receptor 21 deletion improves insulin sensitivity in diet-induced obese mice. *J. Clin. Invest.* 2012; 122:2444–2453. [PubMed: 22653059]

**Figure 1.**

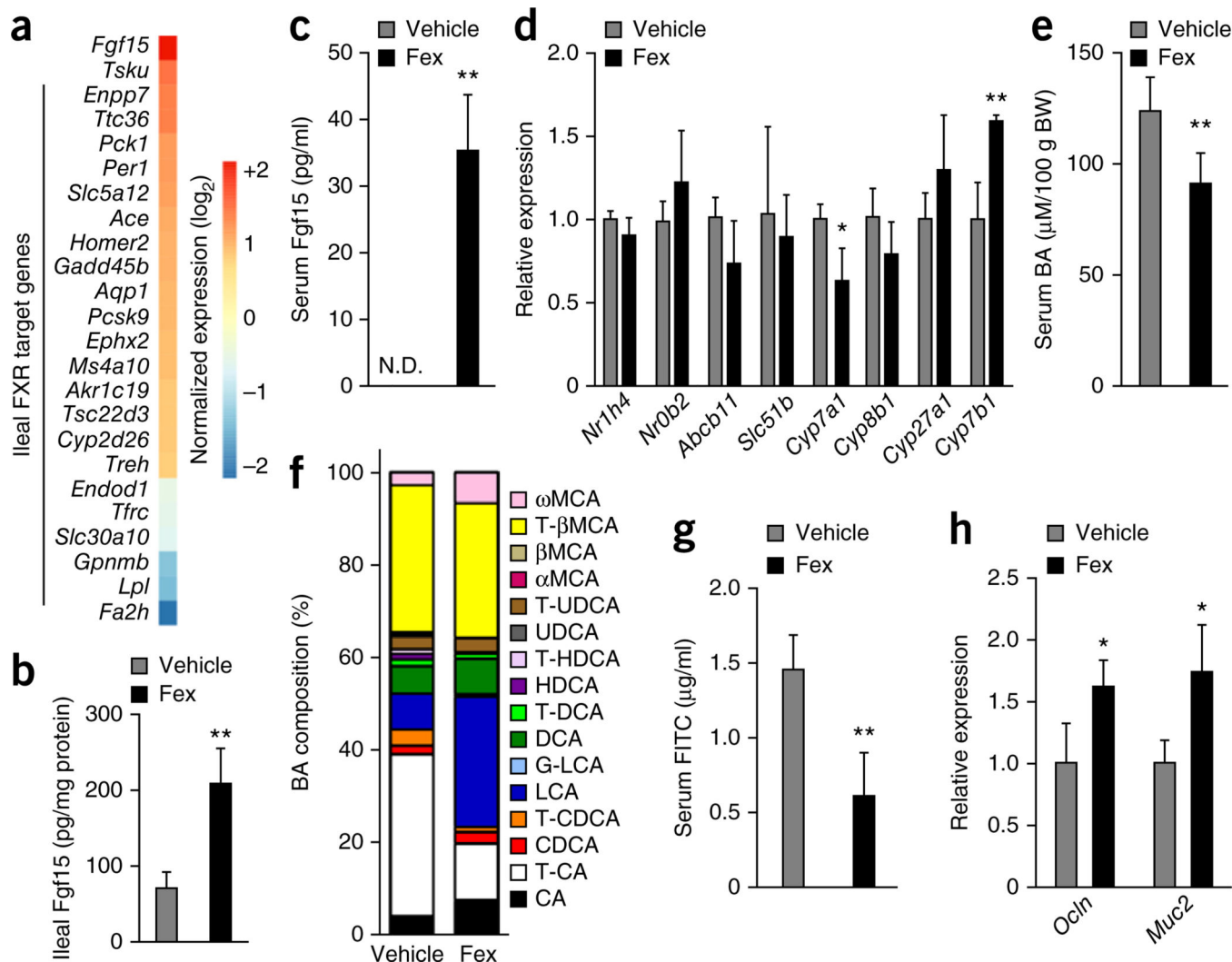
Orally delivered Fex is an intestine-restricted FXR agonist. **(a)** Scheme for determining serum concentrations of Fex. Mice were treated daily with vehicle or Fex ( $100 \text{ mg kg}^{-1}$ ) by p.o. gavage or i.p. injection for 5 d, with tissues and serum collected 1 h after the final treatment. **(b)** Serum Fex concentrations from **a**. **(c)** Relative induction of the canonical FXR target gene SHP in tissues with abundant FXR expression after p.o. or i.p. delivery of Fex, compared with vehicle. **(d)** Induction of FXR target genes in intestine, liver and kidney after p.o. Fex treatment (8-week-old mice treated daily for 3 d  $100 \text{ mg kg}^{-1}$ ). Data are mean  $\pm$  sd. Statistical analysis was done using Student's unpaired *t*-test. \* $P < 0.05$ , \*\* $P < 0.01$ .  $n = 3\text{--}5$  per group.



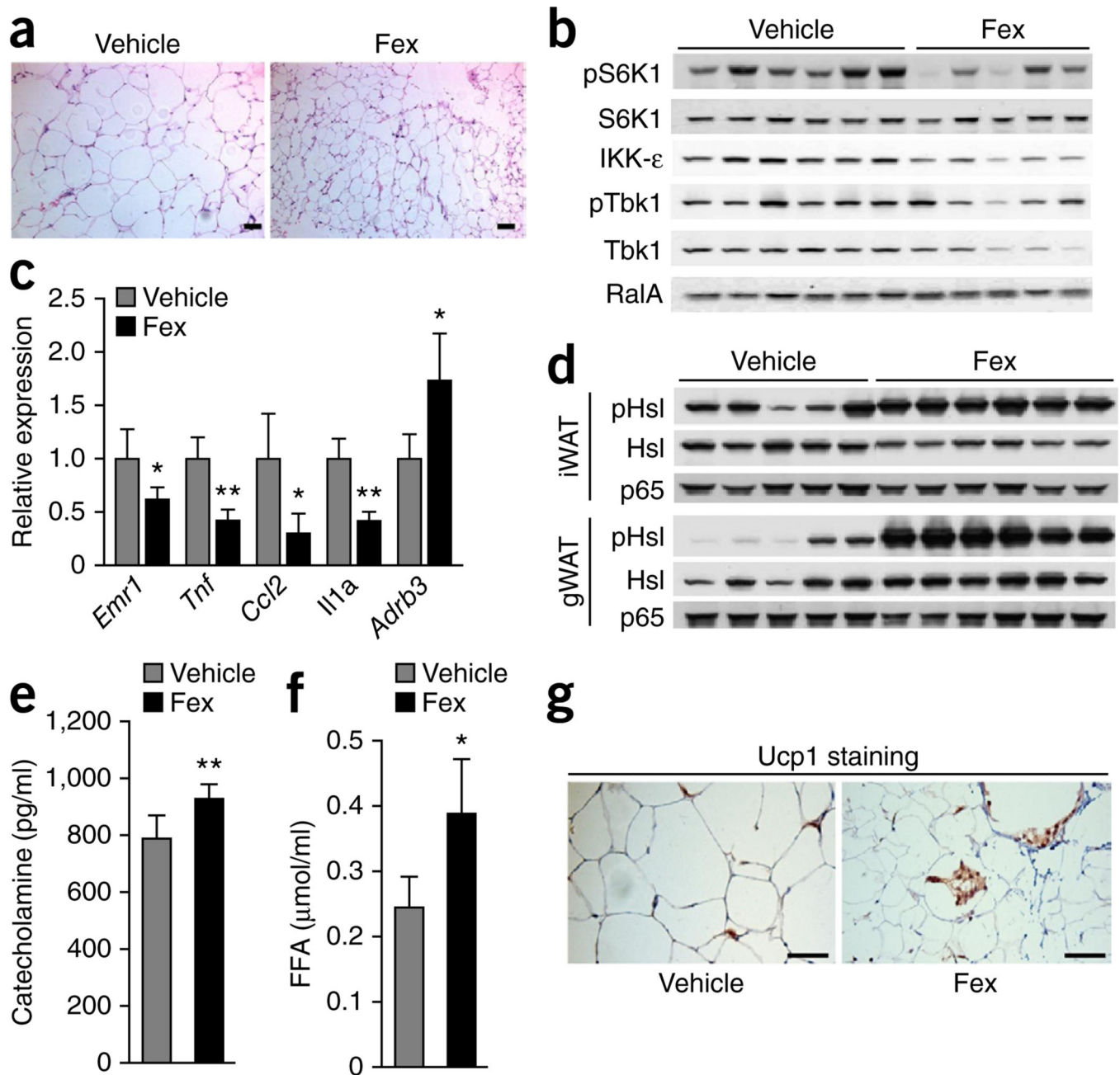
**Figure 2.** Fex prevents diet-induced obesity and improves metabolic homeostasis. Mice fed control or an HFD for 14 weeks were chronically treated with vehicle or Fex ( $100 \text{ mg kg}^{-1} \text{ d}^{-1}$  p.o. for 5 weeks,  $n = 6-8$  per group). **(a)** Body weights. **(b)** Body composition by magnetic resonance imaging. **(c)** Wet weight of inguinal WAT (iWAT), gonadal WAT (gWAT) and mesenteric WAT (mWAT), liver, kidney, heart and spleen. **(d)** Serum parameters after 8-h fast. TG, triglycerides. **(e)** Serum cytokines. **(f)** Glucose tolerance test. **(g)** Insulin tolerance test. Data are mean  $\pm$  sd. Statistical analysis was done using Student's unpaired  $t$ -test.  $*P < 0.05$ ,  $**P < 0.01$ .



**Figure 3.** Fex increases oxidative phosphorylation to enhance metabolic rate in BAT. Mice fed an HFD for 14 weeks were chronically treated with vehicle or Fex (100 mg kg<sup>-1</sup> d<sup>-1</sup> p.o. for 5 weeks,  $n = 6-8$  per group). **(a)** Daily food intake during first week of treatment. **(b)** Carbon dioxide production. **(c)** Oxygen consumption. **(d)** Cumulative ambulatory counts. **(e)** Core body temperature. **(f)** Representative images (three total images per group) of H&E staining of BAT. **(g)** Relative mRNA expression of selected nuclear receptors and genes involved in mitochondrial biogenesis and fatty acid oxidation in BAT. **(h)** Quantification of phosphorylated p38 in BAT. Scale bars, 50 μm. Data are mean ± sd. Statistical analysis was done using Student's unpaired *t*-test. \* $P < 0.05$ , \*\* $P < 0.01$ .



**Figure 4.** Fex increases endogenous Fgf15 signaling and alters serum BA composition. Mice fed an HFD for 14 weeks were chronically treated with vehicle or Fex (100 mg kg<sup>-1</sup> d<sup>-1</sup> p.o. for 5 weeks, *n* = 6–8 per group). (a) Expression of direct FXR target genes in ileum. (b) Fgf15 protein in ileum. (c) Serum Fgf15 levels. (d) Expression of hepatic genes involved in BA metabolism. (e,f) Serum BA levels (e) and composition ratio (f). BW, body weight. (g,h) Intestinal permeability (g) and mucosal defense gene expression (h) in ileum. Scale bars, 50 μm. Data are mean ± sd. N.D., not determined. Statistical analysis was done using Student's unpaired *t*-test. \**P* < 0.05, \*\**P* < 0.01.

**Figure 5.**

Fex reduces inflammation and increases lipolysis in adipose tissues. Mice fed an HFD for 14 weeks were chronically treated with vehicle or Fex (5 weeks of 100 mg kg<sup>-1</sup> d<sup>-1</sup> p.o. delivery, *n* = 6–8 per group). **(a)** Representative images (three total images per group) of H&E staining of mWAT. **(b)** Protein expression levels in gWAT. **(c)** Gene expression of inflammatory cytokines and β-adrenergic receptor in gWAT. **(d)** Protein expression levels of Hsl (pHsl) in gWAT and inguinal WAT (iWAT). **(e)** Serum catecholamine levels. **(f)** Serum FFA levels. **(g)** Representative images (three total images per group) of Ucp1 staining in

iWAT. Scale bars, 50  $\mu\text{m}$ . Data are mean  $\pm$  sd. Statistical analysis was done using Student's unpaired *t*-test. \**P* < 0.05, \*\**P* < 0.01.

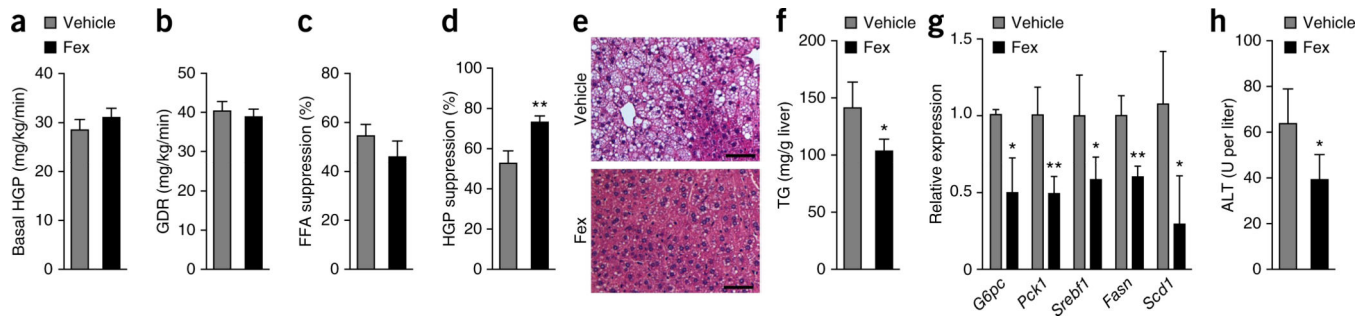


**Figure 6.**

Fex treatment improves glucose homeostasis. (a–d) Hyperinsulinemic-euglycemic clamps performed on weight-matched mice fed an HFD chronically treated with vehicle or Fex (3 weeks of  $100 \text{ mg kg}^{-1} \text{ d}^{-1}$  p.o. delivery,  $n = 12\text{--}14$  per group). (a) Basal HGP. (b) GDR. (c) Percentage FFA suppression by insulin. (d) HGP suppression by insulin. (e–h) Mice were fed an HFD for 14 weeks, after which they were subjected to daily p.o. injection of vehicle or Fex ( $100 \text{ mg kg}^{-1}$ ) for 5 weeks with HFD ( $n = 6\text{--}8$  per group). (e) Representative images (three total images per group) of liver H&E staining. (f) Hepatic triglyceride (TG) levels. (g) Relative mRNA expression of hepatic genes involved in gluconeogenesis and lipogenesis. (h) ALT (alanine aminotransferase) serum levels. Scale bars,  $50 \mu\text{m}$ . Data are mean  $\pm$  sd. Statistical analysis was done using Student's unpaired  $t$ -test. \* $P < 0.05$ , \*\* $P < 0.01$ .